Supplementary Information

Three-Step Thermodynamic vs. Two-Step Kinetic-Limited Sulfur Reactions in All-Solid-State Sodium Batteries

Tongtai Ji[1], Qingsong Tu[2], Yang Zhao,[3] Dominik Wierzbicki[4], Vincent Plisson[5], Ying Wang[1], Jiwei Wang[1], Kenneth S. Burch[5], Yong Yang[6], Hongli Zhu[1,*]

[1]Department of Mechanical and Industrial Engineering, Northeastern University, 360 Huntington Avenue, Boston, Massachusetts 02115, United States

[2]Department of Mechanical Engineering, Rochester Institute of Technology, Rochester, NY 14623, USA

[3]Department of Mechanical and Materials Engineering, University of Western Ontario, London, Ontario N6A 5B9, Canada

[4]National Synchrotron Light Source II, Brookhaven National Laboratory, Upton, NY, 11973 USA

[5]Department of Physics, Boston College, Chestnut Hill, Massachusetts 02467, United States

[6]State Key Laboratory of Physical Chemistry of Solid Surfaces, College of Materials, Xiamen University, Xiamen 361005, China

*: Corresponding author: Hongli Zhu. E-mail: h.zhu@neu.edu

Supplementary Discussion 1

Discussion of the decomposition of the solid electrolyte

In the all-solid-state batteries with sulfide-based SE, it is common that the decomposition of the sulfide-based SE occurs when it intimately contacts with carbon, but the decomposition products are highly reversible during cycling and further protect the unreacted SE.[1,2] The decomposition became obvious when the cells were operated at a slow rate and high temperature. The slow rate and high temperatures under the high voltage (> 2.5V) provide sufficient time and energy for the SE decomposition reaction to take place, resulting in this additional oxidation peak. Supplementary Fig. 4 shows the CV curve of the Na_3PS_4 SE when it intimately contacts with carbon at 90 °C. We also evaluated the capacity provided by the catholyte by mixing SE with the PPCF (85:15) as the cathode material, and the specific capacity of the catholyte is around 40-60 mAh/g with high reversibility (Supplementary Fig. 5). Although the decomposition cannot be avoided, it can be effectively limited by controlling the interface between SE and carbon.[2,3] In our work, for the preparation of the composite cathode (S: C: SE= 35: 15: 50), sulfur was first coated on the PPCF by the melting method and further mixed with the SE to minimize the interface between carbon and SE. Based on the capacity ratio from the catholyte, we expect that less than 5% of the total capacity is contributed by the SE decomposition even at 90°C. This number can be even lower at 25°C. Therefore, the decomposition of the solid electrolyte will not alter the electrochemical behavior of the sulfur cathode we are studying.

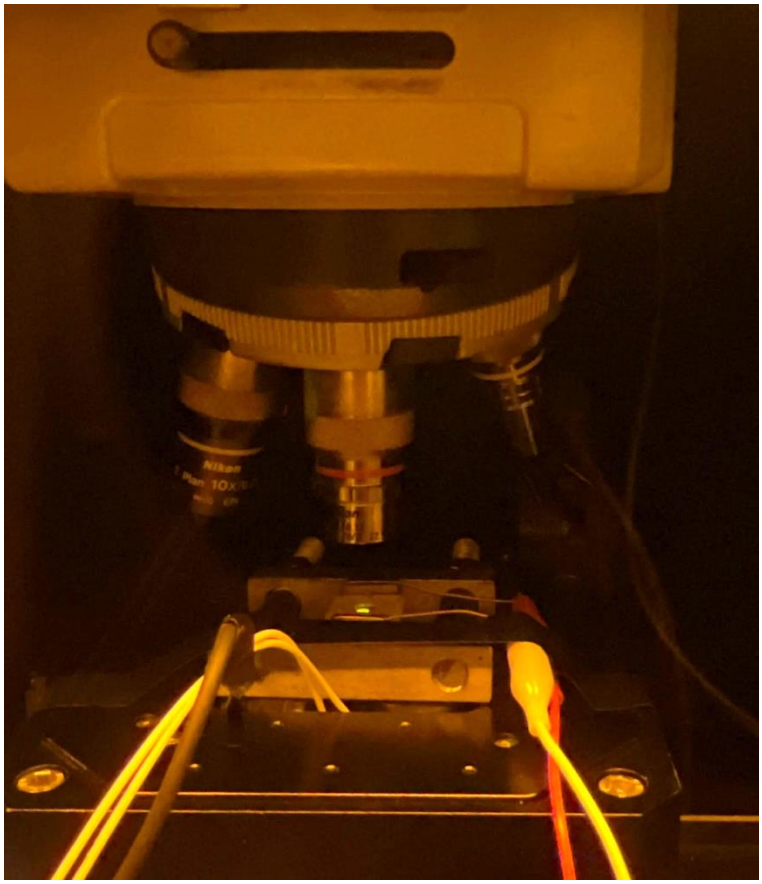

Figure S1. Digital image of the setup for the in-situ Raman test in the glovebox

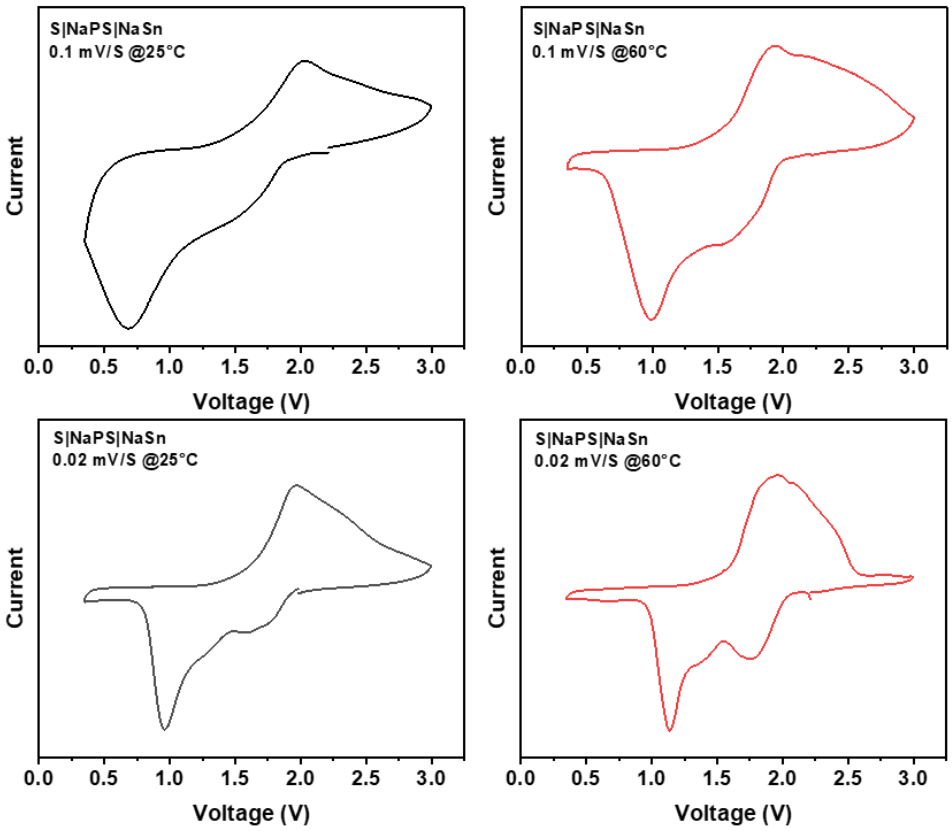

Figure S2. Cyclic voltammetry (CV) curves of the all-solid-state sodium-sulfur batteries operated at 25°C (black), 60°C (red) at 0.1 mV/s (up) and 0.02 mV/s (bottom).

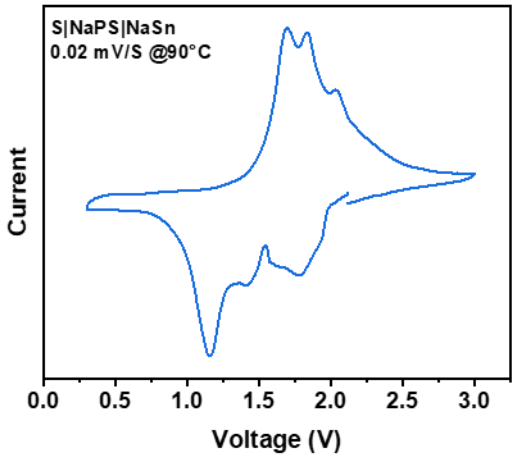

Figure S3. CV curves of the all-solid-state sodium-sulfur batteries operated at 90°C under 0.02 mV/s

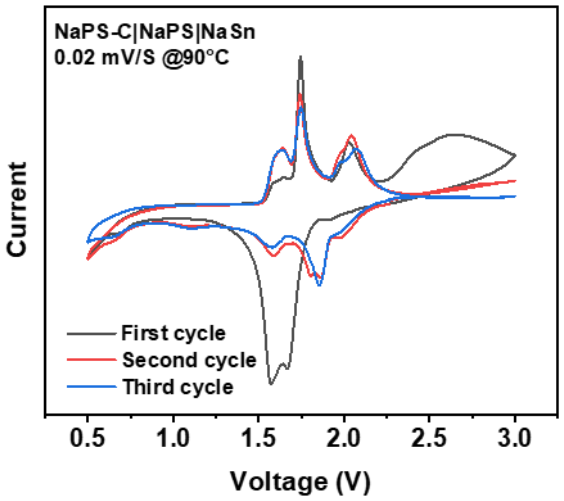

Figure S4. The CV curves of Na_3PS_4 solid electrolyte at 90°C

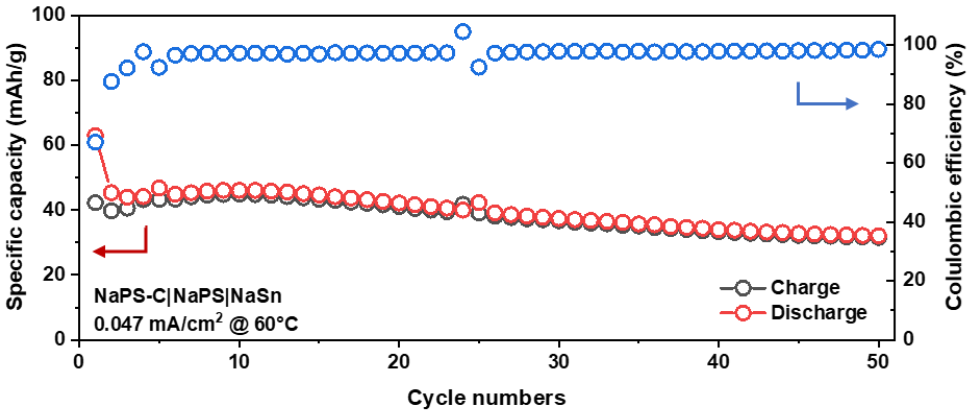

Figure S5. Cycling capacity of the all-solid-state battery with Na_3PS_4 (mixing with PPCF) as the cathode material at 60°C.

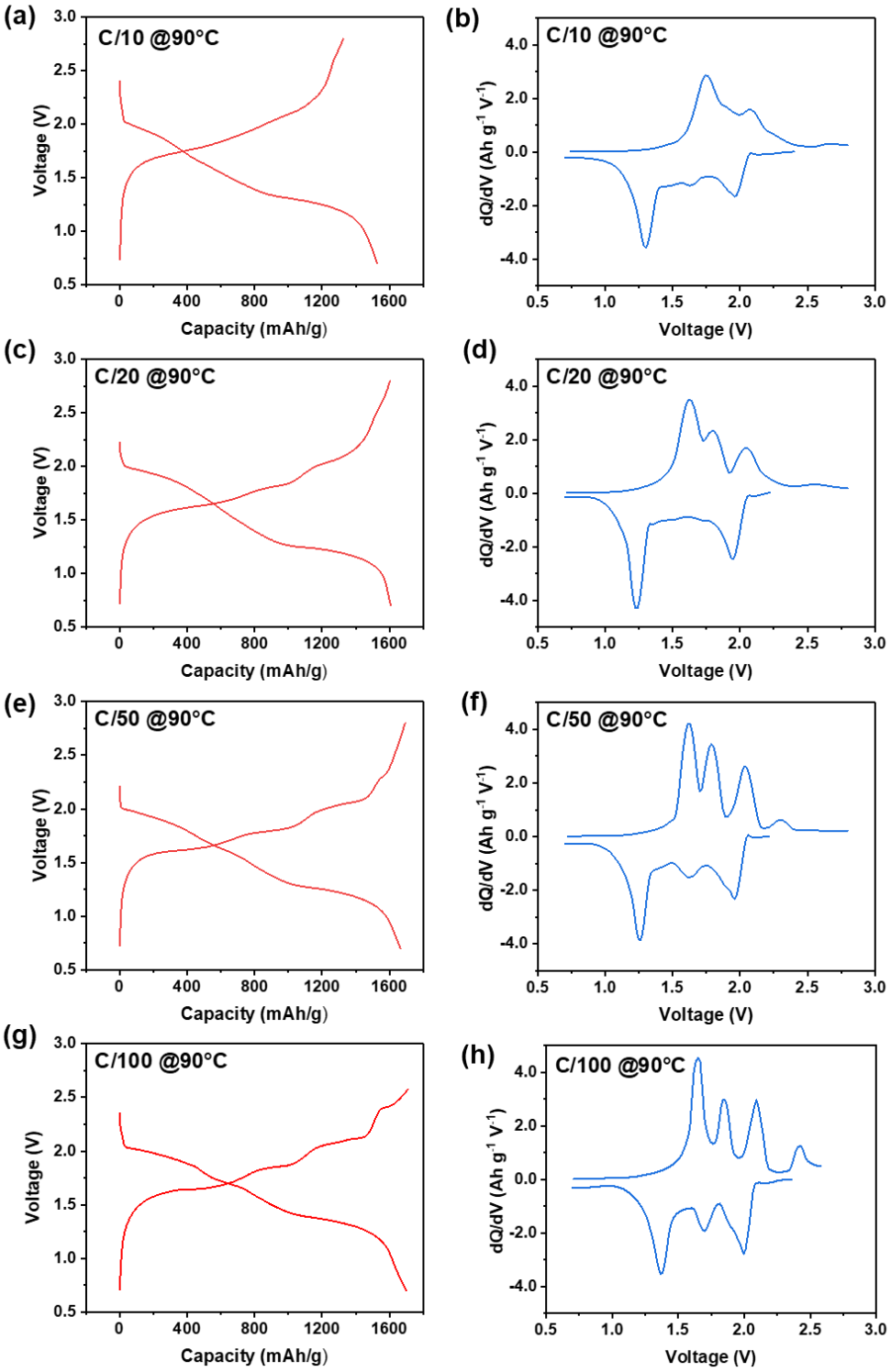

Figure S6. The comparison of the galvanostatic voltage profiles of the all-solid-state sodium sulfur batteries at 90°C under (a) C/100, (c) C/50, (e) C/20, and (g) C/10 and corresponding dQ/dV curves under (b) C/100, (d) C/50, (f) C/20, and (h) C/10.

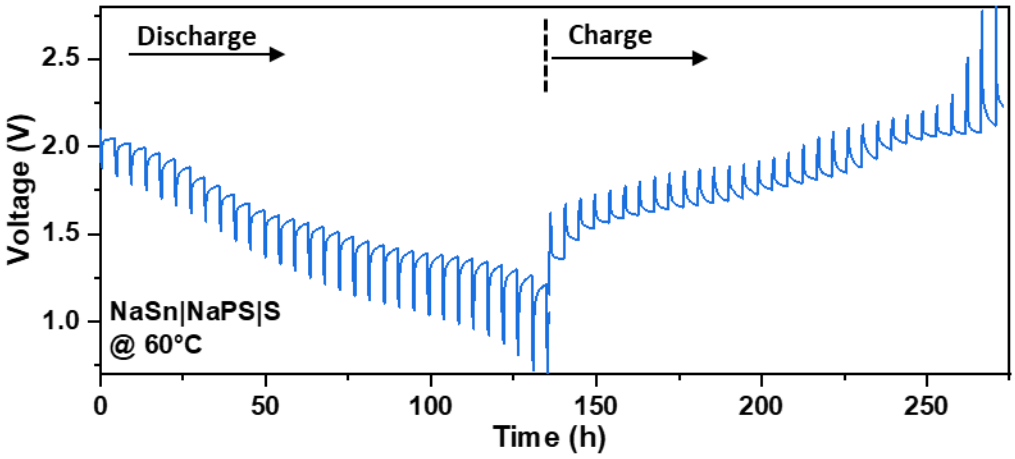

Figure S7. Galvanostatic intermittent titration technique (GITT) test profile of the ASSSBs operated at 60°C.

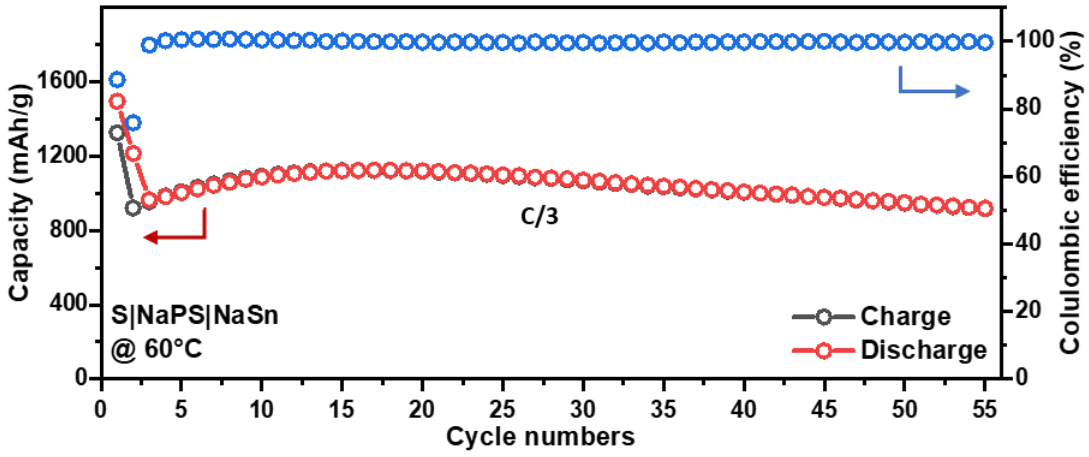

Figure S8. The long cycling performance of the ASSSB operated at 60°C.

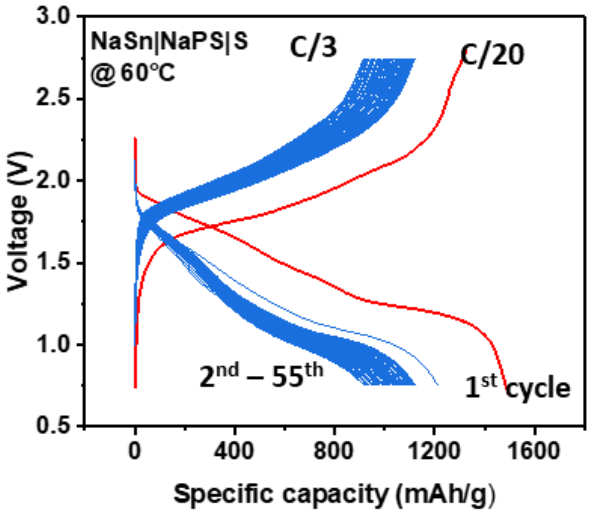

Figure S9. Voltage profiles of the long cycling performance of the ASSSB operated at 60°C.

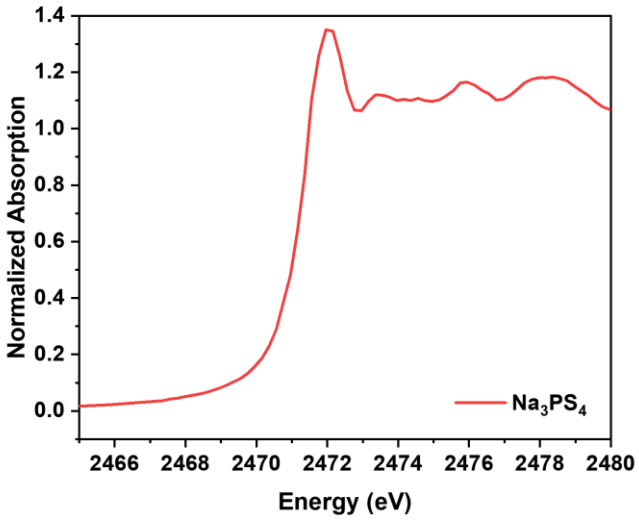

Figure S10. S K-edge XANES spectrum of Na_3PS_4

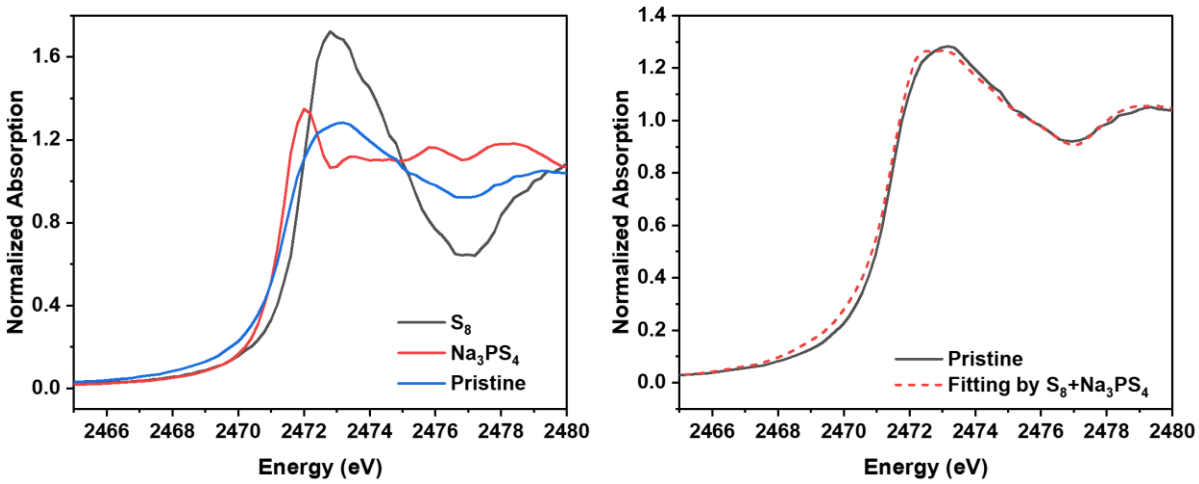

Figure S11. (Left) The comparison of the S K-edge XANES spectra of S_8, Na_3PS_4, and Pristine cathode. (Right) The linear combination fitting result of the pristine cathode by S_8 and Na_3PS_4.

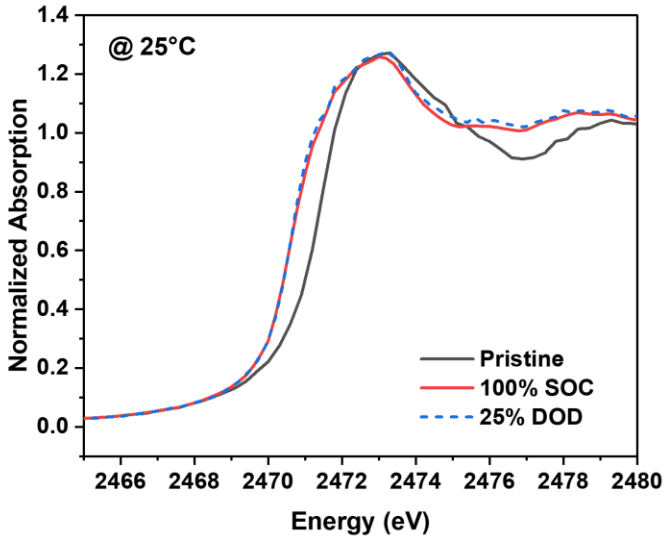

Figure S12. The comparison of the Pristine, 25% DOD, and 100% SOC S K-edge XANES spectra at 25°C.

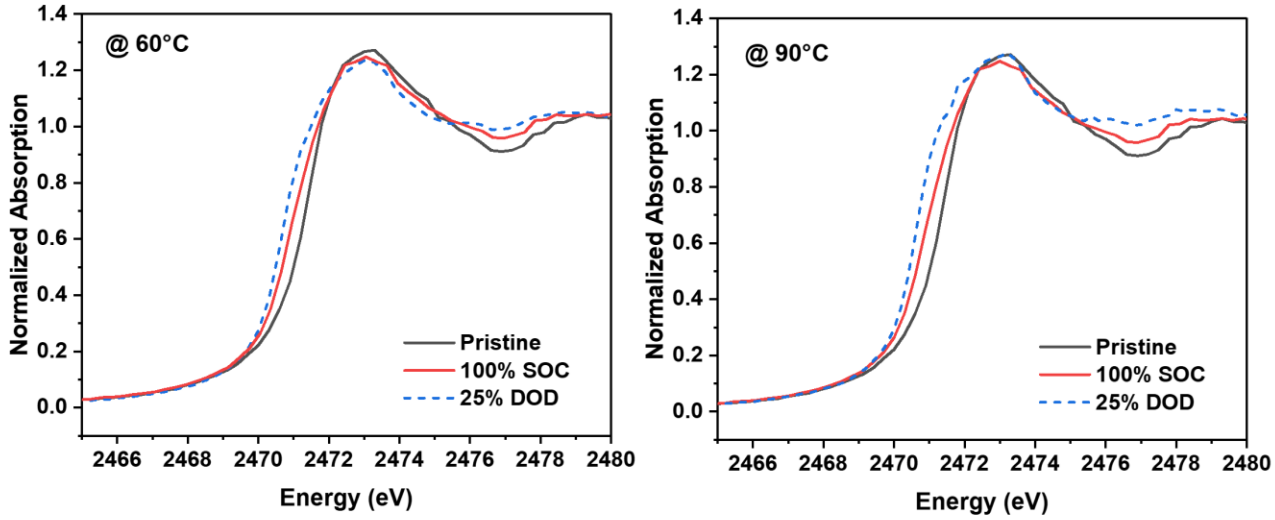

Figure S13. The comparison of the Pristine, 25% DOD, and 100% SOC S K-edge XANES spectra at 60°C (left) and 60°C (right).

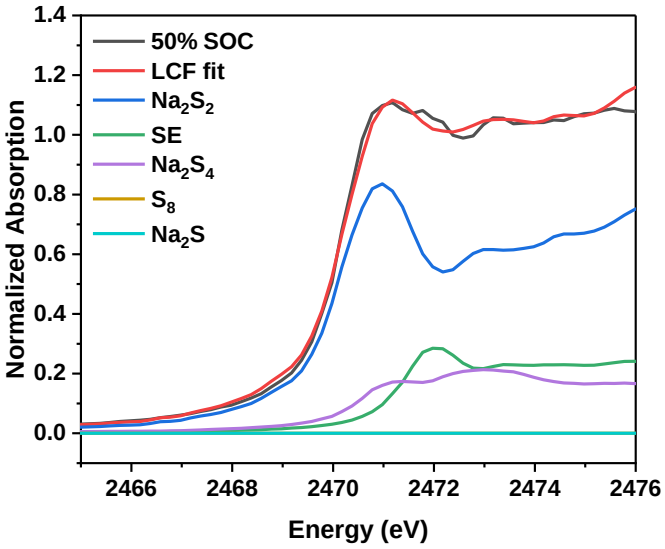

Figure S14. Linear combination fitting (LCF) result of the XANES spectrum of the 50% SOC at 90°C and the reference spectra plotted by the weight of their contributions.

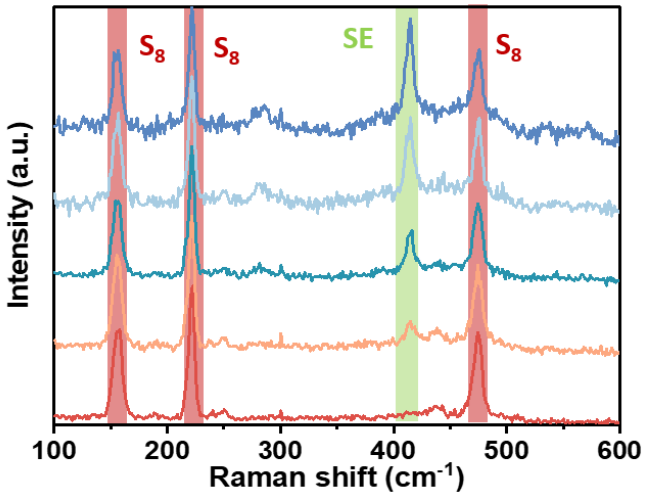

Figure S15. Raman spectrum of the pristine composite cathode at different places.

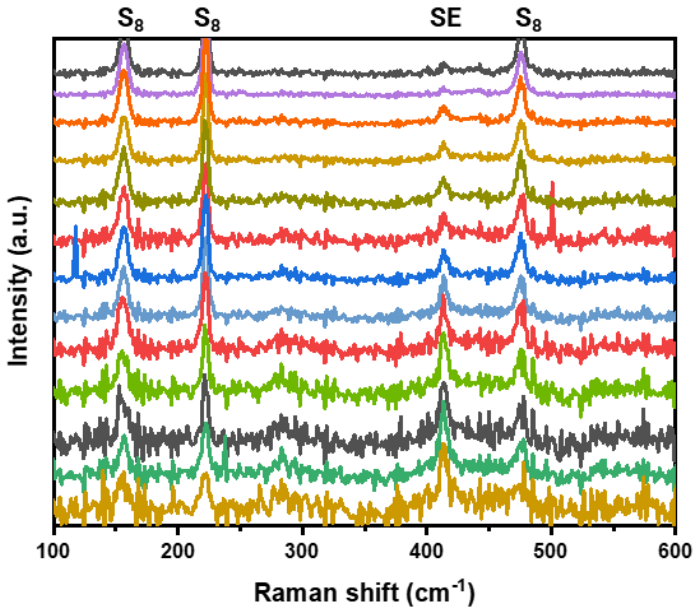

Figure S16. Operando Raman measurement for the most surface layer of the sulfur cathode from 0 to 3h, the change of the sulfide species are hard to detect. The change of the intensity of the peaks from S_8 and SE is due to the slight moving of the position.

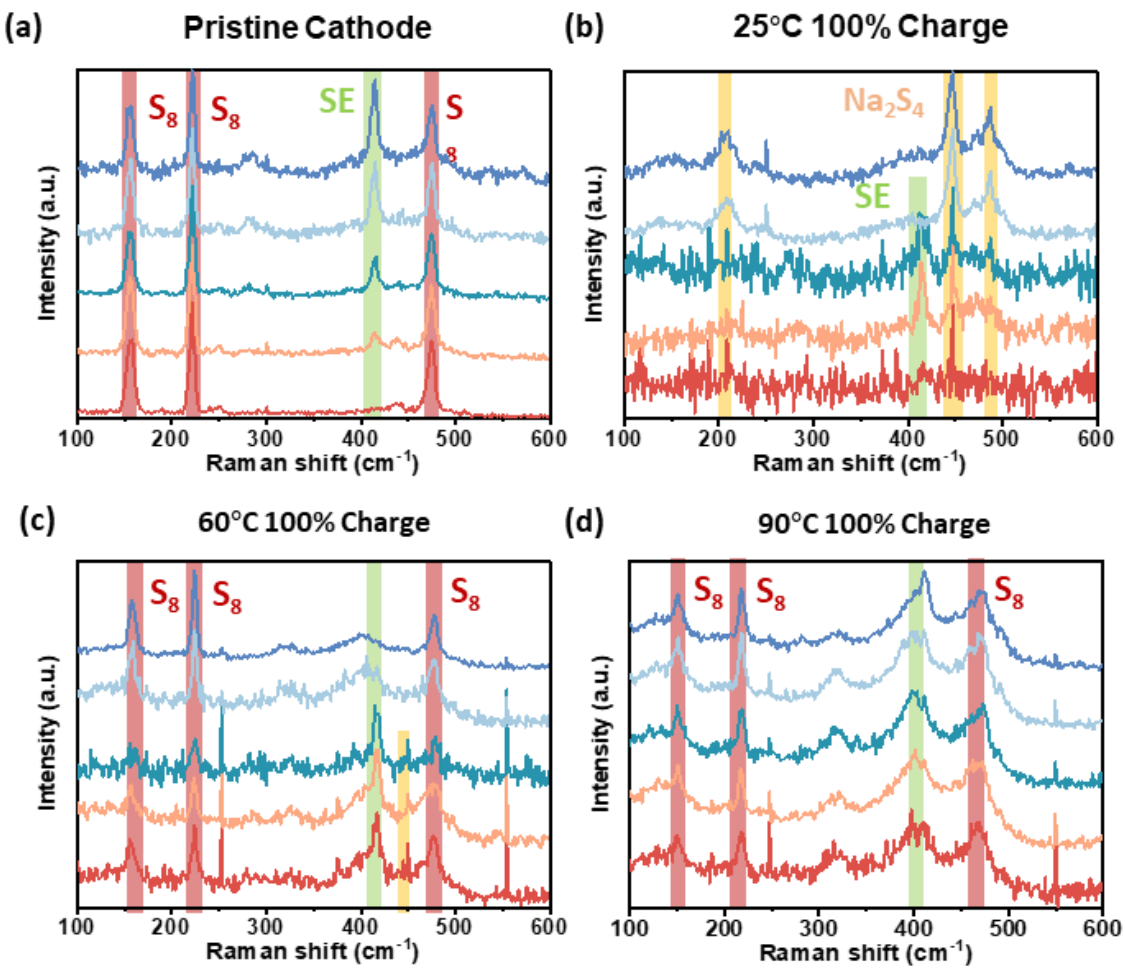

Figure S17. Comparation of the ex-situ Raman spectra of (a) pristine cathode, and the cathode at 100% SoC operated at (b) 25°C, (c) 60°C, and (d) 90°C

Table S1. Lattice constants of different phases

Phase	a constant (Å)	b constant (Å)	c constant (Å)	volume (Å^3/atom)
4(S8)	8.507	8.507	13.551	27.560
4(Na_2S_5)	5.784	7.677	14.529	23.041
4(Na_2S_4)	8.952	8.952	8.952	22.414
2(Na_2S_2)	4.443	4.443	10.205	21.810
Na_2S	4.601	4.601	4.601	22.954
Na_2	3.730	3.730	6.099	36.738

Equation S1. Diffusion coefficient calculated by GITT test[4]

$$\boldsymbol{D = \frac{4}{\pi\tau}\left(\frac{n_m V_m}{S}\right)^2\left(\frac{\Delta E_s}{\Delta E_t}\right)^2}$$

Where, τ (s) is the duration of the current pulse; n_m (mol) is the number of moles of the active material; V_m (cm^3/mol) is the molar volume of the electrode; S (cm^2) is the electrode area; ΔE_s (V) is the steady-state voltage change, due to the current pulse and ΔE_t (V) is the voltage change during the constant current pulse, excluding the iR drop.

Reference

1 Yue, J. *et al.* High-performance all-inorganic solid-state sodium–sulfur battery. *ACS nano* **11**, 4885-4891 (2017).

2 Banerjee, A., Wang, X., Fang, C., Wu, E. A. & Meng, Y. S. Interfaces and interphases in all-solid-state batteries with inorganic solid electrolytes. *Chemical reviews* **120**, 6878-6933 (2020).

3 Tan, D. H. *et al.* Elucidating reversible electrochemical redox of Li6PS5Cl solid electrolyte. *ACS Energy Letters* **4**, 2418-2427 (2019).

4 Jia, M. *et al.* Re-understanding the galvanostatic intermittent titration technique: Pitfalls in evaluation of diffusion coefficients and rational suggestions. *Journal of Power Sources* **543**, 231843 (2022).